Electrical Properties of the Square-Antiprismatic Chain Compounds M_4Br_4Os (M = Y, Er) and M_4Te_4Z (M = Nb, Ta; Z = Si, Cr, Fe, Co)

Kyungsoo Ahn, Timothy Hughbanks,* K. D. D. Rathnayaka, and D. G. Naugle

Department of Chemistry and Department of Physics, Texas A&M University, College Station, Texas 77843

Received September 29, 1993. Revised Manuscript Received January 24, 1994®

The resistivities of the rare-earth metal halides, R_4Br_4Os (R = Y, Er) and several of the ternary tellurides M_4Te_4Z (M = Nb, Z = Si, Fe, Co; M = Ta, Z = Si, Cr, Co) were measured using standard four-probe ac and dc techniques at temperatures ranging from 4.2 to 350 K. The rare-earth halides R_4Br_4Os show semiconducting behavior: conductivity increases exponentially with temperature. Activation energies (E_a) for conduction in Y_4Br_4Os and Er_4Br_4Os are 0.16 and 0.11 eV, respectively. The resistivity of Er_4Br_4Os is 2 orders of magnitude smaller than that of Y_4Br_4Os at 273 K. The behavior of these compounds is in accord with the calculated band structure presented. The isoelectronic compounds M_4Te_4Si (M = Ta, Nb) behave as electronic conductors at high temperature. Ta_4Te_4Si shows a resistivity maximum at 160 K and below 60 K exhibits a broad metal–insulator transition. The absolute resistivity measured for Ta_4Te_4Si is 2 orders of magnitude higher than the other tellurides. The analogue Nb_4Te_4Si shows a similar anomalous resistivity maximum near 280 K and at low temperature (~60 K) exhibits a gradual rise in resistivity that suggests a semiconducting ground state. Transition-metal-centered M_4Te_4Z compounds all behave as simple metals in the temperature range 4.2–300 K; metal–insulator transitions are not seen at temperatures greater than 4.2 K. Nb_4Te_4Fe shows a small resistivity anomaly near 25 K.

Introduction

Over the past 20 years, much study has been devoted to the properties of structurally anisotropic tantalum and niobium chalcogenides. These low-dimensional compounds show interesting physical properties associated with superconductivity or charge-density waves (e.g., MMo_3X_3 (M = alkali metal; X = S, Se, Te),[1] $HfTe_5$ and $ZrTe_5$,[2] $NbSe_3$[3]). More recently, several metal-rich ternary compounds have been prepared in which the third element (Fe, Co, Ni, Si, etc.) serves as an interstitial that resides within an early transition metal cage. Variations in structures and properties accompany variations in ternary elements: in the $Ta_9M_2S_6$ (M = Fe, Co, Ni) series, the Fe- and Co-containing compounds are distorted,[4,5] a resistivity anomaly is found in the cobalt-containing member of the $Ta_{11}M_2Se_8$ (M = Fe, Co, Ni) series;[6,7] and $NbMTe_2$ (M = Fe, Co)[8] are also distinct (the compounds have similar but different structures and differing temperature dependent resistivities).

DiSalvo and co-workers recently reported the synthesis and structure of Ta_4Te_4Si,[9] a compound that bears some structural resemblance to the binary compounds Ta_2S,[10] Ta_3S_2,[11] and the ternary compounds MMo_3X_3 (M = alkali metal; X = S, Se, Te).[1,12-15] As a group, these compounds comprise a series that are built up from trigonal ($Mo_3Te_3^-$), tetragonal (Ta_4Te_4Z), and pentagonal (Ta_3S_2) antiprismatic chains of metal. Figure 1 shows a (001) projection of the Ta_4Te_4Si. Ta_4Te_4Si is one congener of a group of isotypic compounds, Ta_4Te_4Z (Z = Si, Cr, Fe, Co, and Ni) that consist of chains built up from stacked Z-centered square antiprisms of tantalum surrounded by tellurium. These chains propagate up the crystallographic *c* axis and interact with each other via van der Waals interactions. The tellurium atoms are situated so as to bridge each edge of tantalum squares and reside quite near to the plane of the Ta_4 square.

More recently Dorhout and Corbett reported compounds, R_4Br_4Os (R = Y, Er),[16] which are formally isoelectronic with Ta_4Te_4Si and which show a clear structural similarity to the telluride compounds. The structures of these rare-earth compounds consist of chains of condensed rare-earth square antiprisms that are centered by osmium and have bromides that cap the trigonal faces of the antiprisms and serve to cross-link the chains into a three-dimensional array. A (001) projection of the R_4Br_4Os structure is shown in Figure 2. This projection, when compared to the projection depicted in Figure 1,

* Address correspondence to this author at the Chemistry Department.
® Abstract published in *Advance ACS Abstracts,* March 1, 1994.

(1) Tarascon, J. M.; DiSalvo, F. J.; Waszczak, J. V. *Solid State Commun.* **1984**, *52*, 227.
(2) Okada, S.; Sambongi, T.; Ido, M. *J. Phys. Soc. Jpn.* **1980**, *49*, 839.
(3) Rouxel, J. *Acc. Chem. Res.* **1992**, *25*, 328–336.
(4) Harbrecht, B.; Franzen, H. F. *J. Less-Common Met.* **1985**, *113*, 349.
(5) Harbrecht, B. *J. Less-Common Met.* **1986**, *124*, 125.
(6) Harbrecht, B. *J. Less-Common Met.* **1988**, *141*, 59.
(7) Ahn, K.; Hughbanks, T. *J. Solid State Chem.* **1993**, *102*, 446.
(8) Li, J.; Badding, M. E.; DiSalvo, F. J. *Inorg. Chem.* **1992**, *31*, 1050.
(9) Badding, M. E.; DiSalvo, F. J. *Inorg. Chem.* **1990**, *29*, 3952.
(10) Franzen, H. F.; Smeggil, J. G. *Acta Crystallogr. Sect. B* **1969**, *25*, 1736.
(11) Kim, S.-J.; Nanjundaswamy, K. S.; Hughbanks, T. *Inorg. Chem.* **1991**, *30*, 159.
(12) Potel, M.; Chevrel, R.; Sergent, M.; Armici, J. C.; Decroux, M.; Fischer, O. *Acta Crystallogr., Sect. B* **1980**, *B36*, 1545.
(13) Potel, M.; Chevrel, R.; Sergent, M. *J. Solid State Chem.* **1980**, *35*, 286.
(14) Vassiliou, J. K.; Ziebarth, R. P.; DiSalvo, F. J.; Rosenberg, A. *Chem. Mater.* **1990**, *2*, 738.
(15) Tarascon, J. M.; DiSalvo, F. J.; Chen, C. H.; Carroll, P. J.; Walsh, M.; Rupp, L. *J. Solid State Chem.* **1985**, *58*, 290.
(16) Dorhout, P. K.; Corbett, J. D. *J. Am. Chem. Soc.* **1992**, *114*, 1697.

0897-4756/94/2806-0418$04.50/0

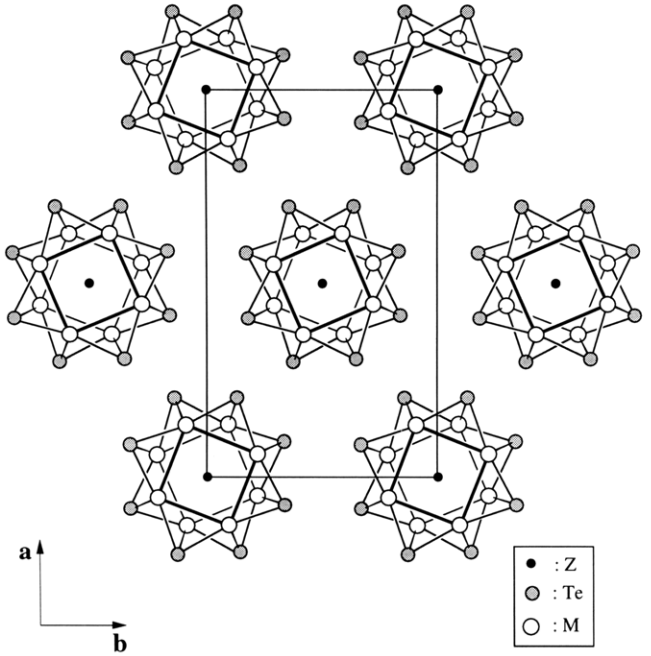

Figure 1. (001) projection of the M_4Te_4Z (M = Ta, Nb; Z = Si, Cr, Fe, Co, Ni) structure.

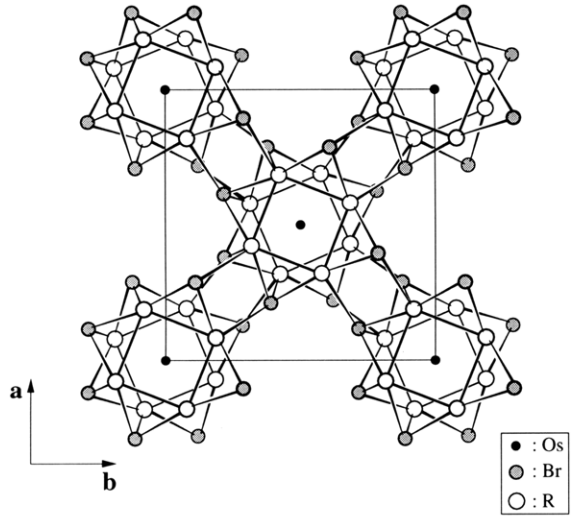

Figure 2. (001) projection of the R_4Br_4Os (R = Y, Er) structure.

makes clear the structural similarity between the rare-earth systems and the group V tellurides. However, there are several important differences between the bromide compounds and the tellurides. Most obviously, the chains in Ta_4Te_4Si are isolated, while those in Y_4Br_4Os are cross-linked via Y–Br bonds. In Figure 3, the two chains are viewed side-by-side. In Ta_4Te_4Si, the tellurides sit on the same planes as the Ta_4 squares and are bonded to four Ta centers, two bonds are made to Ta atoms on the same plane, and one bond is made to metals on each of the adjacent planes (Ta–Te distances: 2×3.25 Å, 2×2.98 Å); in Y_4Br_4Os, the bromides move off the Y_4 planes and are coordinated to only three yttrium centers on the chain but they are also bound to one yttrium on a neighboring chain. There are also important differences between the two rare earth compounds and the group V tellurides in the stacking distances between adjacent M_4 squares. In the Ta_4Te_4Z compounds, the chains are stacked with relatively short interlayer Ta_4–Ta_4 distances (the mean interlayer distance for all Z ranges from 2.39 to 2.43 Å), and this means that Z–Z distances are correspondingly

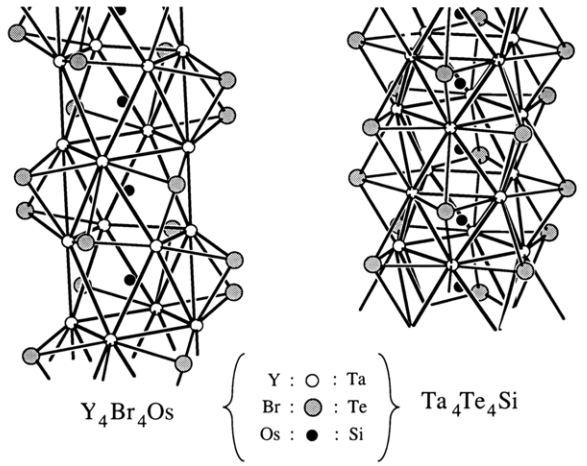

Figure 3. Chains from (a) Y_4Br_4Os and (b) Ta_4Te_4Si. These chains are linked via Y–Br bonds in the former and remain isolated in the latter. The chain axis lattice parameter is much longer in the yttrium compound (see text).

short enough to imply significant Z–Z bonding. In contrast, the mean distance between Y_4 planes in Y_4Br_4Os is 3.28 Å, this is very nearly equal to the Os–Os separation and rules out strong direct Os–Os bonding. The bromides in Y_4Br_4Os are asymmetrically placed around the chain, in one layer bromides cap four adjacent yttrium triangles and in the neighboring layers the opposite four triangles are capped. This asymmetric bromide capping is accompanied by a tilting ($\approx$4°) of the Y_4 squares of the alternating layers of the chain such that the triangles capped by bromides are smaller than the uncapped triangles.

In this paper, we report on our study of the electrical properties of these chain compounds. We use extended Hückel tight-binding calculations[17,18] to aid in understanding the results obtained, and to illuminate the reasons underlying the systematic differences, in the behavior exhibited by the rare-earth halides and the group five tellurides. Our research has also revealed some qualitative differences between the transition metal centered M_4Te_4Z chain compounds and those centered by silicon.

Experimental Methods

Sample Preparation. R_4Br_4Os (R = Y, Er) single crystals were grown in vapor-phase transport reactions from R, RBr_3 and Os powders. Reactions are run at 1050 °C for 3 weeks and then quenched to room temperature. Small needle-shaped crystals were obtained. All rare-earth halide reactions were run under argon inside welded niobium tubes that were jacketed in evacuated silica tubes.

Ta_4Te_4Si single crystals are synthesized by heating stoichiometric ratios of the elemental powders in silica vessels with $TeCl_4$ used as a transport reagent. Following the method of Badding and DiSalvo, samples were heated and kept at 600 °C for 1 day and then at 1100 °C for 2 days and were then quenched rapidly to the room temperature.[9] Nb_4Te_4Si was obtained from the elements by the same method. However, other transition metal ternary tellurides M_4Te_4Z (M = Ta, Z = Cr, Co; M = Nb, Z = Fe, Co) were obtained at 750 °C; above 750 °C attack of the silica container was observed. In these systems, crystal growth was observed at temperatures as low as 600 °C. Reactions were run at 750 °C for 3 days and then rapidly quenched to room temperature.

Characterization. The identities of product phases were verified by powder X-ray diffraction measurements obtained with

(17) Hoffmann, R. *J. Chem. Phys.* **1963**, *39*, 1397.
(18) Whangbo, M.; Hoffmann, R. *J. Am. Chem. Soc.* **1978**, *100*, 6093.

an Enraf-Nonius (FR-552) vacuum Guinier camera using monochromated Cu $K\alpha_1$ radiation. All crystals studied invariably formed with an extreme needlelike habit, and we assume that the needle axes were coincident with crystal axes along which the chains of these one dimensional compounds grow, as we have observed with similar systems.[7] For these materials, crystals grow as exceedingly thin fibers, and scattering was insufficient to observe layer lines even with very long exposure times.

Wavelength-dispersive X-ray spectrometry (WDS) analyses were performed using a Cameca SX50 scanning electron microscope for Ta_4Te_4Co and Ta_4Te_4Cr samples with Ta_2S and Ta, Co, Cr, Si, and Sb_2Te_3 single crystals as calibration standards. Energy dispersive X-ray spectrometry (EDS) was performed on Ta_4Te_4Co, Ta_4Te_4Cr, Ta_4Te_4Si, Nb_4Te_4Fe, Nb_4Te_4Co, and Nb_4Te_4Si samples using a JEOL 6400 scanning electron microscope with Nb, Ta, Si, Co, Sb_2Te_3, and magnetite (Fe_2O_3; 43.7 at. % Fe, 56.3 at. % O) as calibration standards.

Electrical Resistivity Measurements. Four-probe ac resistivities of the halides and the tellurides were measured at a frequency of 25 Hz with an HP 4192A impedance analyzer; standard techniques were used for four-probe dc measurements. Since these compounds are extremely air-sensitive and moisture-sensitive, every measurement was carried out under an inert atmosphere, with the sample contained within a sealed brass container (heat-sink). All measurements were repeated at least twice on separate crystals.

Silver epoxy (Acme E-solder 3021) was used to make all contacts to halide crystals, and leads from the contacts were made with 0.05-mm-diameter gold wires. (In–Ga alloys were observed to react with the rare-earth halides soon after contact was made.) For the halides, temperature-dependent measurements were taken over the range 160–273 K. Er_4Br_4Os crystals were too small to attach four probes and so data for this compound is derived from two probe measurements. For Y_4Br_4Os, vapor-phase transport synthesis afforded crystals that were long enough to attach four probes (0.7 mm); the flux method originally reported by Dorhout and Corbett did not produce sufficiently long crystals for resistivity measurements.[16] Two-probe ac measurements were also collected over the same temperature range for comparison with two-probe measurements on Er_4Br_4Os.

Resistivities of Ta_4Te_4Z (Z = Si, Cr, Co) and Nb_4Te_4Z (Z = Si, Fe, Co) were measured by four-probe dc techniques between temperatures of 4.2 and 350 K. The resistivities of tellurides were measured while both cooling and warming and showed no "thermal hysteresis", indicative of good temperature equilibration throughout the period of measurement. For the computation of absolute resistivities, the needlelike crystals' cross sections were measured with a Zeiss laser scanning microscope (LSM-10). Crystal dimensions for resistivities reported herein were 0.04 mm × 0.04 mm × 0.7 mm (Y_4Br_4Os), 0.025 mm × 0.025 mm × 0.3 mm (Er_4Br_4Os), 3.5 μm × 3.5 μm × 1 mm (Ta_4Te_4Si), 1 μm × 1 μm × 1.2 mm (Ta_4Te_4Cr), 5 μm × 5 μm × 0.8 mm (Ta_4Te_4Co), 3.8 μm × 3.8 μm × 1.2 mm (Nb_4Te_4Si), 2.3 μm × 2.3 μm × 1 mm (Nb_4Te_4Fe), 1.5 μm × 1.5 μm × 1.3 mm (Nb_4Te_4Co).

Results and Discussion

Dorhout and Corbett reported the crystallization of the rare-earth metal halides R_4Br_4Os (R = Y, Er) from a NaBr flux.[16] In contrast, we obtain single crystals of these halides that were long enough (0.7–0.8 mm) for conductivity measurements from vapor phase transport (VPT) reactions. For each compound, powder diffraction data indicate no sign of any phases but the intended product. In a manner analogous to that of Badding and DiSalvo, we obtain the ternary telluride Ta_4Te_4Si and Nb_4Te_4Si crystals by VPT from stoichiometric reactions in which a trace (≈1 mg) of $TeCl_4$ was used as a transport agent.[9] However, other ternary isostructural compounds were synthesized at 750 °C and then annealed in sealed Ta or Nb tubes in evacuated silica vessels. Each of the compounds forms crystals that are very anisotropic fibers, with widths from 0.7 to 3 μm and lengths of up to 5 mm.

Table 1. Cell Parameters for Compounds Studied

	cell parameters			
compounds	a, Å	b, Å	c, Å	β, deg
Ta_4Te_4Si[a]	10.545(2)	18.301(3)	4.8034(8)	
Ta_4Te_4Cr	10.545(4)	18.325(10)	4.823(2)	
Ta_4Te_4Fe	10.544(5)	18.350(13)	4.824(3)	
Ta_4Te_4Co	10.511(6)	18.234(12)	4.791(3)	
Nb_4Te_4Si	10.518(4)	18.240(8)	4.836(5)	
Nb_4Te_4Fe	10.465(3)	18.190(6)	4.845(2)	
Nb_4Te_4Co	10.470(2)	18.158(6)	4.820(1)	
Y_4Br_4Os[b]	12.526(2)	12.392(2)	6.5756(6)	90.86(2)
Er_4Br_4Os[b]	12.446(3)	12.326(3)	6.4973(7)	90.88(1)

[a] Lattice parameters from a single-crystal of Ta_4Te_4Si published in ref 9 were systematically smaller: a = 10.536(3), b = 18.275(5), c = 4.799(1) Å. [b] Lattice parameters from Guinier powder diffraction patterns in ref 16: Y_4Br_4Os: a = 12.514(5), b = 12.381(4), c = 6.672(2) Å, β = 90.96(3)°. Er_4Br_4Os: a = 12.434(5), b = 12.321(3), c = 6.492(1) Å, β = 90.92(3)°.

We synthesized single crystals of Ta_4Te_4Z and Nb_4Te_4Z (Z = Cr, Fe, Co), and X-ray powder patterns verified that these compounds are isostructural with Ta_4Te_4Si. However, these crystals were too thin to scatter X-rays to the extent necessary for X-ray single-crystal structure determinations. The lattice parameters of these compounds are shown in Table 1. Cell parameters from Guinier powder diffraction patterns of R_4Br_4Os (R = Y, Er) are close to those originally reported,[16] though our parameters show somewhat greater precision and exhibit a very small systematic deviation ($\sim 3\sigma$). Since silicon is a potential contaminant in Ta_4Te_4Z and Nb_4Te_4Z phases where Z is a transition metal (the silica container may serve as a source for compounds prepared at temperatures near 1000 °C), analyses of these samples are important. Quantitative analyses (WDS) for bulk samples of Ta_4Te_4Co and Ta_4Te_4Cr gave compositions of $Ta_{4.07}Te_{3.85}Co_{1.06}$ and $Ta_{3.89}Te_{4.07}Cr_{1.03}$. The range of inhomogeneity in the bulk samples was typically 5% for Te and Ta and up to 10% for Co or Cr. We think that nonstoichiometry in these compounds is structurally unlikely and that such inhomogeneities are due to unidentified binary phases in bulk samples. EDS analyses of other materials indicated no detectable unintended elements. Most important, microprobe analyses indicated no detectable silicon contamination in all transition-metal-centered chain compounds discussed herein.

Figure 4 clearly shows the conductivity of the rare-earth halides R_4Br_4Os (R = Y, Er) to be thermally activated. The linear plots of log σ vs $1/T$ demonstrate that the conductivity of these compounds varies exponentially with the negative inverse temperature—in accordance with the semiconducting behavior predicted from band structure calculations (see below). Limitations of crystal size prevented us from performing four-probe resistivity measurements on Er_4Br_4Os, but the reproducibility of our two-probe (ac) measurements for this compound and the similarity between the behavior of Er_4Br_4Os and Y_4Br_4Os indicate that contact resistance does not significantly affect the temperature dependence measured. The slopes of these plots yield activation energies for conduction of 0.16 eV for Y_4Br_4Os and 0.11 eV for Er_4Br_4Os, and the resistivity of the Er compound is smaller than that of Y_4Br_4Os by 2 orders of magnitude (assuming that the two-probe measurements can be so compared). Fortunately, we could obtain needlelike crystals of Y_4Br_4Os that were long enough for four-probe measurements; the ac conductivity was measured by both four-probe and two-probe methods.

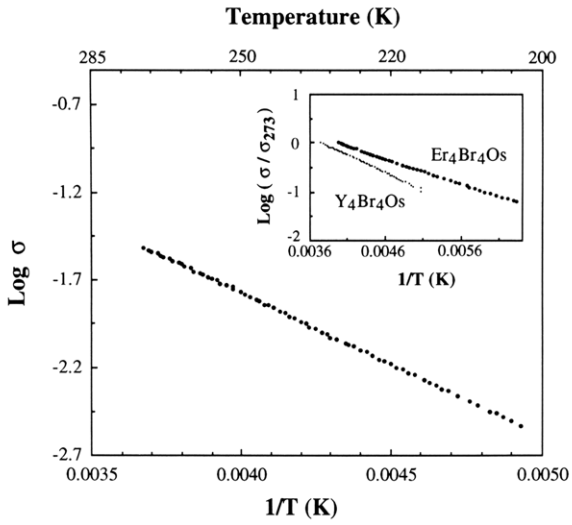

Figure 4. Temperature dependence of the single-crystal conductivities for the R_4Br_4Os (R = Y, Er) systems. The inset shows the results of two-probe measurements for both systems; the four-probe measurements for Y_4Br_4Os are given in the main plot.

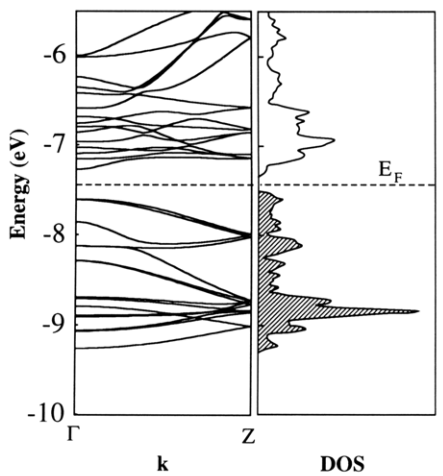

Figure 5. (a, left) Band dispersion curves for Y_4Br_4Os plotted for a line in the Brillouin zone parallel to the chain axis (Γ to *Z*: k = (0,0,0) to (0,0,π/a)). (b) Density of states for Y_4Br_4Os. Note the deep minimum in the DOS near the Fermi level. The energy range encompasses only the metal d bands.

The semiconducting behavior exhibited by Y_4Br_4Os and Er_4Br_4Os are nicely accounted for by the results of band structure calculations. The extended Hückel method was used to obtain the results in Figures 5 and 6; parameters and computational details are given in the Appendix. At left in Figure 5 we show dispersion curves for the Y_4Br_4Os d-bands plotted along a line in the Brillouin zone parallel to the chain axes. At right in the same figure, the total density of states (DOS) can be seen as characteristic of a one-dimensional system—peaks in the DOS clearly correspond to the flat regions of the bands plotted at left. Occupied bands are shown as shaded in the DOS; the Fermi level lies in a 0.18-eV gap that corresponds to a small gap in the curves plotted at left. If the Y_4Br_4Os system was perfectly one-dimensional and there was *no* dispersion in the bands normal to the chain axis, then the dispersion curves at left in Figure 5 would have a gap equal to that seen in the DOS. As it happens, the gap is narrowed by band dispersion normal to the chain axis.

A plot of the band dispersions (in the d-band energy range) in any direction normal to the chain axis reveals the bands to be quite flat, as expected for this anisotropic

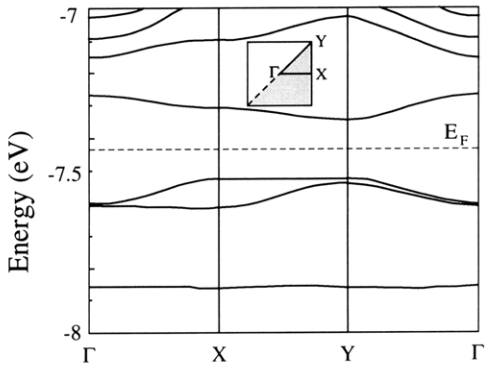

Figure 6. Dispersion curves for Y_4Br_4Os are plotted for lines in the Brillouin zone normal to the chain axis (Γ to *X*: k = (0,0,0) to (π/*a*,0,0); *X* to *Y*: k = (π/a,0,0) to (π/a,π/b,0)). The Fermi level is depicted as a dashed line at −7.43 eV. These lines are indicated in the inset; the shaded region of this slice through the Brillouin zone indicates the irreducible wedge of the zone that was used in the DOS calculation (Figure 5).

system. As a result, the only region of k space where any crossings between the valence and conduction band can occur is in the k_z = 0 plane because that is where the valence and conduction bandgap is smallest in the one-dimensional plot (we take z to be parallel to the chain axis; the k_z = 0 plane corresponds to the Γ point in the one-dimensional plot at left in Figure 5). Figure 6 shows the band dispersion curves plotted over some selected lines in the k_z = 0 plane for the 1-eV energy range including the Fermi level. As the figure indicates, we calculate no crossing between the valence and conduction bands, and the bandgap is 0.18 eV (at the point Y). It should be noted that the accuracy of our method (or any other method capable of handling this complex system) is not sufficient to be certain of the magnitude of the calculated gap—the close correspondence between the calculated 0.18-eV gap and the observed 0.16-eV activation energy found for Y_4Br_4Os is certainly fortuitous. In fact, for an analogous calculation on a hypothetical Y_4Br_4Ru, we calculate a very small valence–conduction band overlap. It should be noted that since the band dispersions in the xy plane are so small, we would expect the effective masses for electron transport (hopping) between chains to be quite large. It is safe to conclude that if there is any overlap between the valence and conduction band, it is quite limited and beyond our method's ability to calculate *and* even if such overlap exists the electron transport it implies is likely to be better described as "hopping conduction" which we would expect to be activated anyway.

Despite their similar structures, the Ta and Nb ternary tellurides have quite different behavior from the rare-earth halides. Figures 7 and 8 show the temperature dependence of the resistivity of Ta_4Te_4Z (Z = Cr, Co) and Nb_4Te_4Z (Z = Fe, Co), respectively. The compounds Ta_4Te_4Z show simple metallic behavior down to 4.2 K. We have measured the resistance of Ta_4Te_4Cr at low temperature using the two-probe dc method. It shows simple metallic behavior and no resistivity anomalies. At 273 K, the resistivity of Ta_4Te_4Cr and Ta_4Te_4Co are 1.8×10^{-3} and 2.3×10^{-3} Ω cm, respectively. Nb_4Te_4Co also shows simple metallic behavior down to 4.2 K with no resisitivity maximum or metal–insulator transition. Nb_4Te_4Fe shows a small resistivity maximum at 25 K and is the best conductor among the tellurides measured.

Figures 9 and 10 show the temperature-dependent resistivities of Ta_4Te_4Si and Nb_4Te_4Si. The temperature

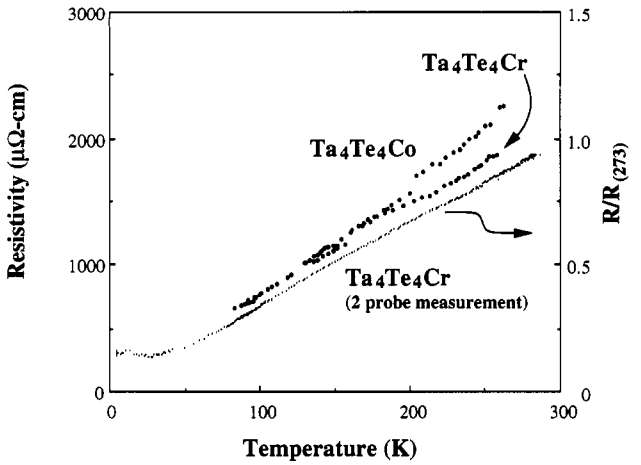

Figure 7. Temperature-dependent single-crystal resistivities for the Ta_4Te_4M (M = Cr, Co) systems are shown.

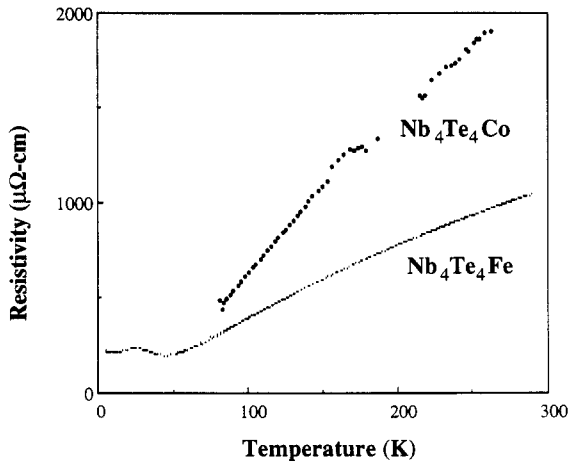

Figure 8. Temperature-dependent single-crystal resistivities for the Nb_4Te_4M (M = Fe, Co) systems are shown.

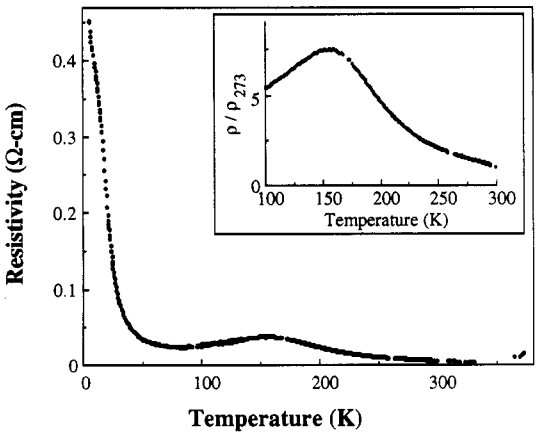

Figure 9. Temperature dependence of the single-crystal resistivity for Ta_4Te_4Si is shown. As explained in the text, the maximum in the resistivity near 170 K is slightly sample dependent.

dependent behavior of Ta_4Te_4Si is dramatically unlike its transition metal-centered congeners. The resistivity at 273 K is an order of magnitude greater than for Ta_4Te_4Cr and Ta_4Te_4Co. The broad maximum seen in the resistivity near 170 K is somewhat sample dependent; we have observed values of $R_{max}/R_{(273)}$ between 4 and 7, with maxima occurring between 165 and 170 K. This variability seems to be reasonably attributed to corresponding variability in defects in this highly anisotropic material.

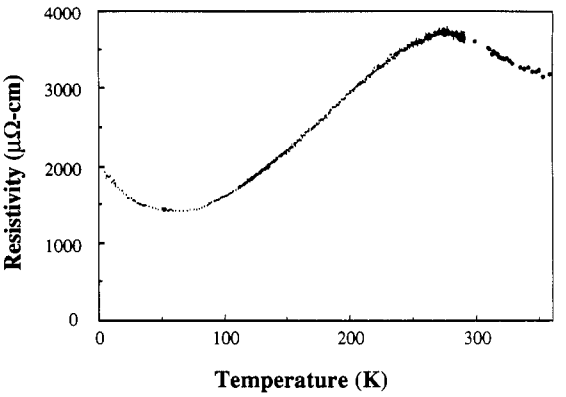

Figure 10. Temperature dependence of the single-crystal resistivity for Nb_4Te_4Si is shown.

The rise in the resistivity seen below 60 K for Ta_4Te_4Si suggests a semiconducting ground state for this system that derives from a Peierls distortion. Nb_4Te_4Si shows behavior that is qualitatively similar to Ta_4Te_4Si, a broad resistivity maximum is found at 280 K, and at ~60 K it exhibits a gradual rise in resistivity that suggests a semiconducting ground state. The behavior of these compounds, especially Ta_4Te_4Si, is phenomenologically reminiscent of $NbSe_3$ for which more dramatic resistivity anomalies are convincingly attributable to charge density waves.[19-21]

While it is natural to assume that the observed resistivity anomaly is attributable to a structural phase transition arising from the strong anisotropy in both the crystallographic and the electronic structure, a tight-binding study of Ta_4Te_4Si gives no clear indication whether CDW behavior is to be expected.[22] In this case, calculations were insufficient to predict whether a distorted structure is more energetically favorable than an undistorted structure. Still, the same calculations clearly indicate that metallic conductivity would be expected for all the Ta_4Te_4Z compounds in the *absence* of CDW behavior, either commensurate (as a Peierls distortion) or incommensurate. In this sense, the contrast between the rare-earth halides and the group V tellurides is predicted by the extended Hückel band calculations.

An indication of a metal–insulator Peierls transition is the presence of a strong peak in the logarithmic derivative of the resistivity as a function of T^{-1}.[23] When so analyzed, our data shows only a broad Gaussian-like peak. Such data are typically sensitive to impurity concentrations because disorder introduced by impurities disrupts the onset of long-range order in the transition. Since our starting materials are susceptible to impurity contamination (especially, Nb in Ta compounds), a more careful study of this system is indicated; a study of several alloy systems ($Ta_{4-x}Nb_xTe_4Si$, $Ta_{4-x}Zr_xTe_4Si$ and $Ta_{4-x}Hf_xTe_4Si$) of these group V ternary tellurides is in progress.

The resistivity maxima of Ta_4Te_4Si and Nb_4Te_4Si are quite similar to behavior observed for $ZrTe_5$ and $HfTe_5$, although the pentatellurides show no low-temperature

(19) Haen, P.; Monceau, P.; Tissier, B.; Waysand, G.; Meerschaut, A.; Molinie, P.; Rouxel, J. *Proc. Fourteenth Int. Conf. Low Temp. Phys.* **1975**, *5*, 445.
(20) Ong, N. P.; Monceau, P. *Phys. Rev. B* **1977**, *16*, 3443.
(21) Ong, N. P.; Brill, J. W. *Phys. Rev. B* **1978**, *18*, 5265.
(22) Li, J.; Hoffmann, R.; Badding, M. E.; DiSalvo, F. J. *Inorg. Chem.* **1990**, *29*, 3943.
(23) Etemad, S.; Engler, E. M.; Schultz, T. D.; Penny, T.; Scott, B. A. *Phys. Rev. B* **1978**, *17*, 513.

metal–insulator transition.[24,25] Whether any phenomenological connection exists between these two classes of compounds remains to be established.

We have not attempted to look for electric field dependence in the resistivity of Ta_4Te_4Si, at least not at low fields. At higher electric fields (10–40 V/cm) non-Ohmic behavior was not seen. Measurements at lower fields (1–10 mV/cm) would be more appropriate to explore possible CDW behavior (as for $NbSe_3$).[26] Finally, we note that preliminary data indicate that Ta_4Te_4Si exhibits interesting magnetoresistance anisotropy which is similar to that exhibited by Ta_3S_2.[27]

Concluding Remarks

The R_4Br_4Os (R = Y, Er) and M_4Te_4Z (M = Ta, Nb; Z = Si, Cr, Fe, Co) systems, despite their structural similarity, have markedly contrasting properties. While the former two compounds are semiconducting with small energy gaps, the tellurides are metallic (at ambient temperature). Among the tellurides, the Si-centered chain systems are the most intriguing, displaying large resistivity anomalies that may be the result of charge density waves. The transition-metal-centered chain systems behave more like conventional metals.

Further investigation of these systems' properties is warranted by the question left unanswered in this paper. More generally, further synthetic investigation and theoretical analysis should enrich our understanding of the structure–property relationships that hold for these metal–metal bonded chain systems. (For example, Llusar and Corbett have very recently reported the existence of R_4I_4Z (R = Sc, Y, Gd, Er; Z = Fe, Ru, Os, Ir) wherein the chains are not cross-linked by R–I bonds like the bromides discussed here. We think it may be very important that the iodides in these phases have a structural role very much like the tellurides discussed here.)[28] The interplay of synthesis, structure, and properties in this area will continue to fascinate us for some time to come.

(24) Wieting, T. J.; Gubser, D. U.; Wolf, S. A. *Bull. Am. Phys. Soc.* **1980**, *25*, 340.
(25) DiSalvo, F. J.; Fleming, R. M.; Waszczak, J. V. *Phys. Rev. B* **1981**, *24*, 2935.
(26) Fleming, R. M.; Grimes, C. C. *Phys. Rev. Lett.* **1979**, *42*, 1423.
(27) Nozaki, H.; Wada, H.; Takekawa, S. *J. Phys. Soc. Jpn.* **1991**, *60*, 3510.
(28) Llusar, R.; Corbett, J. D., submitted for publication.

Table 2. Parameters for EH Calculations

	orbital	H_{ii}, eV	ζ_1[b]	ζ_2[b]	c_1[a]	c_2[a]
Y	4d	−6.80	1.56	3.554	.8316	.3041
	5s	−7.02	1.74			
	5p	−4.40	1.70			
Os	5d	−8.18	2.416	5.57	.6689	.5877
	6s	−5.57	2.45			
	6p	−2.61	2.43			
Br	4s	−28.0	2.64			
	4p	−13.9	2.26			

[a] Coefficients used in double-ζ expansion. [b] Slater-type orbital exponents.

Acknowledgment. Research in the chemistry department (T.H. and K.A.) was generously supported by the National Science Foundation through Grant DMR-9215890 and by the Robert A. Welch Foundation through Grant A-1132. Support for research in the physics department (K.D.D.R. and D.G.N.) was derived from the Robert A. Welch Foundation through Grant A-0514. Work in both the chemistry and physics departments received additional support through an Interdisciplinary Research Initiative award administered by the Texas A&M Office of the Associate Provost for Research and Graduate Studies. We thank Dr. R. N. Guillemette in the Department of Geology at Texas A&M for providing his expertise in microprobe analysis, Yunchao Tian for her help in performing band structure calculations, and Dr. Charles Runyan for early help in the synthesis of the R_4Br_4Os compounds.

Appendix

The extended Hückel method[17,18] was used for band structure calculations on Y_4Br_4Os. Parameters appear in Table 2: parameters for bromine and yttrium were taken from previous work,[29] osmium H_{ii} values are from a previous charge iterative calculation,[29] and osmium exponents are from Basch and Gray.[30] Structural parameters were from reported crystallographic data for Y_4Br_4Os.[16] Band structure calculations were carried out using a 160K point mesh for the 3-D monoclinic cell. DOS curves were smoothed with Gaussian functions with a half-width of 0.025 eV. Dispersion curves for selected lines in the Brillouin zone were obtained by calculation of 50K points per line.

(29) Hughbanks, T.; Corbett, J. D. *Inorg. Chem.* **1989**, *28*, 631.
(30) Basch, H.; Gray, H. B. *Theor. Chim. Acta* **1966**, *4*, 367.